Supporting Information

Zhang et al. 10.1073/pnas.1413210111

SI Experimental Procedures

Animals. All animals (WT, $CB_1^{-/-}$, and $CB_2^{-/-}$) used in these experiments were matched for age (8–14 wk) and weight (25–35 g). The Zimmer $CB_2^{-/-}$ mice (1) are C terminal-deleted. The last 341 base pairs on exon 3 are deleted; these encode parts of the intracellular and extracellular third loops, transmembrane regions 6 and 7, and the intracellular C terminus region.

In Situ Hybridization.

RNA extraction and cDNA synthesis. Approximately 30 mg of tissue was disrupted and homogenized for RNA extraction. Total RNA was isolated from tissue samples using the Qiagen RNeasy Mini Kit following the manufacturer's instructions. cDNA was synthesized from 1 μg of RNA using the Bio-Rad iScript cDNA Synthesis Kit. cDNA was kept at −80 °C until use.

CB_2 mRNA riboprobe synthesis. PCR was performed with Taq DNA polymerase (Roche Applied Science) using CB_2-KO primers (Table S2), and the product (105 bp long) was purified using the Qiagen QIAquick Gel Extraction Kit according to the manufacturer's protocol. The PCR product was then inserted into the plasmid vector (pCR4-TOPO10; TOPO TA Cloning Kit; Life Technologies) and used to transform TOP10 cells (Life Technologies). The plasmid-containing mCB_2R fragment was sequenced using an Applied Biosystems 3130XL Genetic Analyzer. After sequencing, the antisense plasmid and sense plasmid could be picked up, because the PCR products were inserted at random into the plasmid vectors. Computer-assisted homology searches (blast.ncbi.nlm.nih.gov/Blast.cgi) showed that the designed probe recognized both CB_{2A} and CB_{2B} isoforms (2), with no significant homology with the CB_1 receptor or other proteins. The sense and antisense probes for mCB_2Rs were transcribed in vitro with the appropriate RNA polymerases and labeled with digoxigenin-UTP using a Roche digoxigenin RNA labeling kit with T7 RNA polymerase according to the manufacturer's protocol. The synthesized RNA probes were purified with Roche mini Quick Spin RNA columns, and the quality of the synthesis was monitored by dot blot analysis.

Single fluorescent ISH. Nine mice (three animals per strain) were used for ISH. The ISH procedures were carried out in free-floating sections as described previously (3) with minor modifications. In brief, sections were pre-equilibrated in 5× SSC buffer (0.75 M NaCl and 7.5 mM Na citrate) for 10 min and prehybridized in a hybridization solution containing 50% deionized formamide (Sigma-Aldrich), 5× SSC, and 40 μg/mL denatured salmon DNA (Sigma-Aldrich) in H_2O-DEPC at 58 °C for 2 h. Subsequently, the sense and antisense digoxigenin-labeled probes were denatured at 80 °C for 5 min, and then added to the hybridization mix (500 ng/mL), in which the sections were hybridized at 58 °C for 16 h. After washing, sections were further incubated with an alkaline phosphatase-conjugated anti-digoxigenin antibody (1:1,000 in 0.5% BSA TN blocking buffer; Roche) for 1.5 h at room temperature and stained using a Roche HNPP/Fast Red TR fluorescent detection kit. The staining was stopped by repeated washes in a rinsing solution (0.01 M Tris·HCl and 0.001 M EDTA; pH 8.0). The sections were mounted on slides and air-dried.

Dual-fluorescent visualization of CB_2 mRNA and TH expression. To determine the phenotype of mCB_2 mRNA-expressing neurons in the midbrain, we used fluorescent immunohistochemistry (IHC) to label dopaminergic neurons with TH antibody. After the mCB_2 mRNA staining by ISH described above, the sections were incubated with a mouse anti-TH antibody (1:1,000; Millipore) at 4 °C overnight, followed by Alexa Fluor 488 goat anti-mouse IgG (1:500; Molecular Probes) at room temperature for 2 h. The sections were mounted on glass slides, air-dried at room temperature, and coverslipped with Fluorogel with Tris buffer (Electron Microscopy Sciences).

RNAscope ISH Assays. WT and $CB_2^{-/-}$ mice were deeply anesthetized and transcardially perfused with saline. Whole brain tissues were removed and rapidly frozen on dry ice. The fresh-frozen tissue sections (15 μm thick) were mounted on positively charged microscopic glass slides (Fisher Scientific). Both the Cnr2-specific RNA probe (1,877–2,820 bp of the *Mus* Cnr2 mRNA sequence) and the TH RNA probe (483–1,603 bp of the *Mus musculus* TH mRNA sequence) were designed and provided by Advanced Cell Diagnostics. All staining steps were performed following RNAscope protocols (4). Stained slides were coverslipped with fluorescent mounting medium (ProLong Gold Antifade Reagent P36930; Life Technologies) and scanned into digital images with an Olympus FluoView FV1000 confocal microscope at 40× magnification using manufacturer-provided software.

IHC Assays.

CB_2 antibodies. Due to concerns regarding CB_2 antibody specificity and the use of partial $CB_2^{-/-}$ mice, we used three antibodies with epitopes in different receptor regions to detect CB_2 receptor expression in mouse brain:

(*i*) Rat CB_2 antibody (rCB_2-Ab), purchased from Abcam (ab-3561). The epitope is located at the extracellular N-terminal (amino acids 1–32) of the rCB_2 receptor. There are five different amino acid residues in the epitope between rat and mouse CB_2 receptors. We chose this rCB_2-Ab because mouse CB_2 antibodies (mCB_2-Ab) with an epitope at the CB_2 receptor N-terminal are currently unavailable.

(*ii*) mCB_2-Ab, purchased from Alomone (ACR-002), which recognizes the intracellular third loop. The epitope (amino acids 228–242) is identical between rCB_2 and mCB_2 receptors.

(*iii*) NIH5633 mCB_2-Ab (custom-designed), which recognizes the mCB_2 receptor C-terminal. The epitope (326-340 aa) is identical between rCB_2 and mCB_2 receptors. The NIH-5633 antibody was produced by Genemed Synthesis.

The titers of the CB_2 antibodies used in IHC assays were NIH5633 mCB_2-Ab (1:500), Alomone mCB_2-Ab (1:250), and Abcam rCB_2-Ab (1:1,000).

VTA neuron IHC assays. VTA slice preparation was performed as described previously (5). IHC was performed using the anti-TH antibody (1:500) and one of the CB_2 antibodies noted above. After washes, sections were further incubated with a mixture of secondary antibodies: Alexa Fluor 488 goat anti-rabbit for CB_2 receptors and Alexa Fluor 568 goat anti-mouse for TH (1:500) and GFAP (1:500) or CD11b (1:500) in 5% BSA and 0.5% Triton X-100 phosphate buffer for 2 h at room temperature. Sections were then washed, mounted, and coverslipped. Fluorescent images were taken using a fluorescence microscope (Nikon Eclipse 80i) or confocal microscope (Nikon Eclipse C1) equipped with a digital camera. All images were taken under identical optical conditions through 4× to 40× objectives.

To determine whether deletion of CB_2Rs abolished expression of CB_2Rs on VTA DA neurons, densitometric analysis was used to quantify CB_2 immunostaining density on individual VTA DA neurons (6). Each CB_2-positive DA neuron was outlined manually and CB_2 fluorescence intensity was measured with ImageJ software. Background signal was defined as the mean background from 5–10 regions outside of the DA neurons in each

slice. After background subtraction, an F/A ratio was used to define the mean fluorescence of individual DA cells (F) normalized to the total cellular surface (A). Quantification was carried out on more than 100 cells from two to five animals of each strain.

Spleen tissue IHC assays. Mice (n = 4 of each strain) were deeply anesthetized with pentobarbital (100 mg/kg i.p.) and then perfused with 30–50 mL cold saline, followed by 4% paraformaldehyde in 0.1 M phosphate buffer. Whole spleens were then removed and transferred to 20% sucrose in phosphate buffer at 4 °C overnight. Spleen sections were then cut at 12 μm on a cryostat. IHC procedures were identical to those described above.

Electrophysiology Studies.

Patch-clamp recordings in single dissociated DA neurons. Coronal midbrain slices (400-μm thickness) were prepared from 14- to 21-d-old mice (WT and $CB_2^{-/-}$ mice) as described previously (7, 8). Then brain slices were incubated in artificial cerebrospinal fluid containing 1 mg/6 mL pronase (Calchem) at 31 °C for 25–35 min. The VTA area from each slice was then punched out using a well-polished needle punch. Each punched tissue fragment was transferred to a 35-mm culture dish filled with well-oxygenated standard extracellular solution composed of 150 mM NaCl, 5 mM KCl, 1 mM $MgCl_2$, 2 mM $CaCl_2$, 10 mM glucose, and 10 mM Hepes, with pH adjusted to 7.4 with Tris base. Each tissue fragment was then mechanically dissociated using a fire-polished micro-Pasteur pipette. Isolated single cells usually adhered to the bottom of the dish within 30 min and were then used for patch-clamp recording at room temperature within 4 h.

Perforated (amphotericin B) patch-clamp recording was performed in single VTA DA neurons obtained through an enzymatic/mechanical dissociation process as described previously (7, 8). Phenotypic identification of DA neurons was based on three criteria: electrophysiology [DA neurons exhibited low spontaneous FRs (1–3 Hz) with long AP duration and a distinctive H-current], pharmacology (DA neuron firing was inhibited by DA or D_2 receptor agonists), and IHC staining (recorded neurons were TH-positive) (Fig. S6). After stable recording for several minutes (baseline), JWH133 or other drugs were bath-applied to the recorded neuron for 1–2 min and then washed out. Rapid application of drugs was performed using a computer-controlled "U-tube" system that allowed for complete exchange of the solution surrounding the recorded cell within 30 ms. Data were acquired with Clamplex 9.2 (Axon Instruments) via a Digidata 1322 series A/D board set to a sampling frequency of 10 kHz, filtered in Clampfit 9.2 using an eight-pole Bessel filter and a 1-kHz low-pass filter, and stored on hard media for subsequent off-line analysis.

Cell-attached patch-clamp recordings in VTA slices. For slice patch-clamp recordings, horizontal midbrain slices (250 μm thick) were prepared from 14- to 21-d old mice (WT and $CB_2^{-/-}$) as described previously (9). To maintain an intact intracellular environment, we used a cell-attached mode of patch recording. In this way, we were able to measure stable neuronal firing for hours. After recording, we converted from cell-attached mode to conventional whole-cell recording to identify the neuronal phenotype of the recorded neuron according to standard electrophysiological, pharmacologic, and immunostaining criteria as described above (9, 10). The effects of JWH133, AM 630, and other drugs on single DA neuron firing in the VTA were evaluated.

Extracellular single-unit recordings in anesthetized mice. Two-month-old male WT and $CB_2^{-/-}$ mice were used for this experiment. Each mouse was anesthetized with chloral hydrate (300 mg/kg i.p., maintained with supplemental doses administrated via the lateral tail vein) and mounted in a stereotaxic apparatus (Narishige Group). Body temperature was maintained at 36–37 °C with a homeothermic blanket system (Harvard Apparatus). VTA DA neuronal activity was recorded and identified using methods described previously (11, 12). Glass microelectrodes with resistance ranging from 6 to 8 MΩ were filled with 2 M NaCl and 0.1% Chicago blue. The latter was used to verify the recording site in the brain using standard histological procedures after the completion of the experiment. The recording electrode was placed into the VTA through a small burr hole in the skull above the VTA (2.9–3.9 mm posterior to Bregma and 0.2–0.8 mm lateral to the midline) and positioned using a stepping motor micromanipulator (Narishige Group). DA neurons were most often encountered at 3.5–4.2 mm below the cortical surface. Data were collected and analyzed using a data acquisition system at Fudan University (Shanghai, China) and stored in a computer for off-line analysis. To monitor spontaneous neuron firing, each identified DA neuron was recorded for at least 30 min. The effects of JWH133 or AM 630 on VTA DA neuron firing were evaluated.

1. Buckley NE, et al. (2000) Immunomodulation by cannabinoids is absent in mice deficient for the cannabinoid CB(2) receptor. *Eur J Pharmacol* 396(2-3):141–149.
2. Liu QR, et al. (2009) Species differences in cannabinoid receptor 2 (CNR2 gene): Identification of novel human and rodent CB_2 isoforms, differential tissue expression and regulation by cannabinoid receptor ligands. *Genes Brain Behav* 8(5):519–530.
3. Lanciego JL, et al. (2011) Expression of the mRNA coding the cannabinoid receptor 2 in the pallidal complex of *Macaca fascicularis*. *J Psychopharmacol* 25(1):97–104.
4. Wang F, et al. (2012) RNAscope: A novel in situ RNA analysis platform for formalin-fixed, paraffin-embedded tissues. *J Mol Diagn* 14(1):22–29.
5. Bäckman C, et al. (1999) A selective group of dopaminergic neurons express Nurr1 in the adult mouse brain. *Brain Res* 851(1-2):125–132.
6. Viscomi MT, et al. (2009) Selective CB2 receptor agonism protects central neurons from remote axotomy-induced apoptosis through the PI3K/Akt pathway. *J Neurosci* 29(14):4564–4570.
7. Wu J, et al. (2004) Electrophysiological, pharmacological, and molecular evidence for alpha7-nicotinic acetylcholine receptors in rat midbrain dopamine neurons. *J Pharmacol Exp Ther* 311(1):80–91.
8. Yang K, et al. (2009) Distinctive nicotinic acetylcholine receptor functional phenotypes of rat ventral tegmental area dopaminergic neurons. *J Physiol* 587(Pt 2):345–361.
9. Gao M, et al. (2010) Mechanisms involved in systemic nicotine-induced glutamatergic synaptic plasticity on dopamine neurons in the ventral tegmental area. *J Neurosci* 30(41):13814–13825.
10. Yang K, et al. (2011) Functional nicotinic acetylcholine receptors containing α6 subunits are on GABAergic neuronal boutons adherent to ventral tegmental area dopamine neurons. *J Neurosci* 31(7):2537–2548.
11. Gao M, et al. (2007) Functional coupling between the prefrontal cortex and dopamine neurons in the ventral tegmental area. *J Neurosci* 27(20):5414–5421.
12. Zhang D, Yang S, Jin GZ, Bunney BS, Shi WX (2008) Oscillatory firing of dopamine neurons: Differences between cells in the substantia nigra and ventral tegmental area. *Synapse* 62(3):169–175.

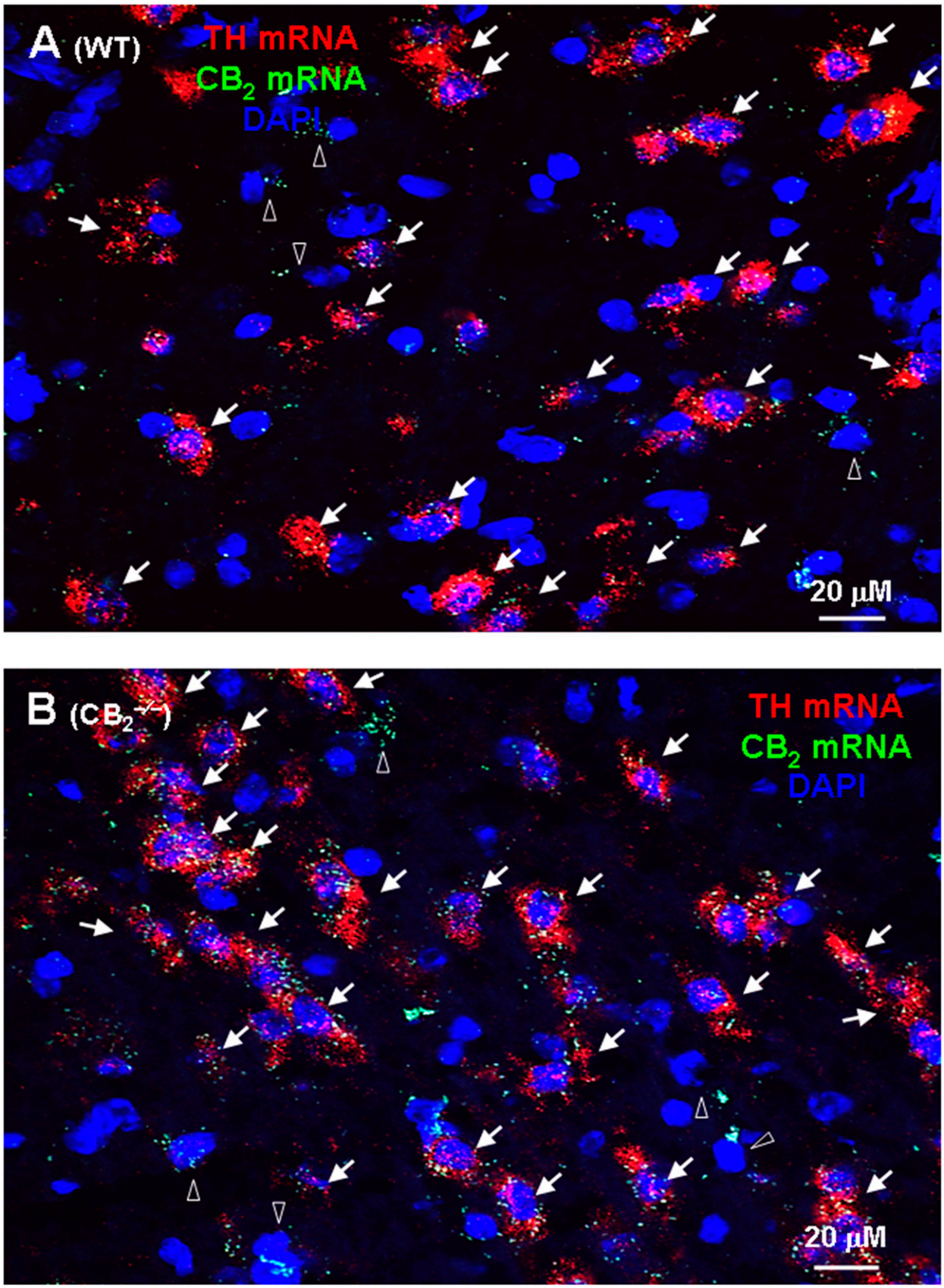

Fig. S1. (Related to Fig. 2.) Representative confocal images under high magnification, illustrating colocalization of CB_2 mRNA (green) and TH mRNA (red) in VTA DA neurons (white arrows) in WT (*A*) and Zimmer $CB_2^{-/-}$ (*B*) mice. CB_2 mRNA is also expressed in TH-negative VTA non-DA neurons (open triangles), as detected by RNAscope ISH assays.

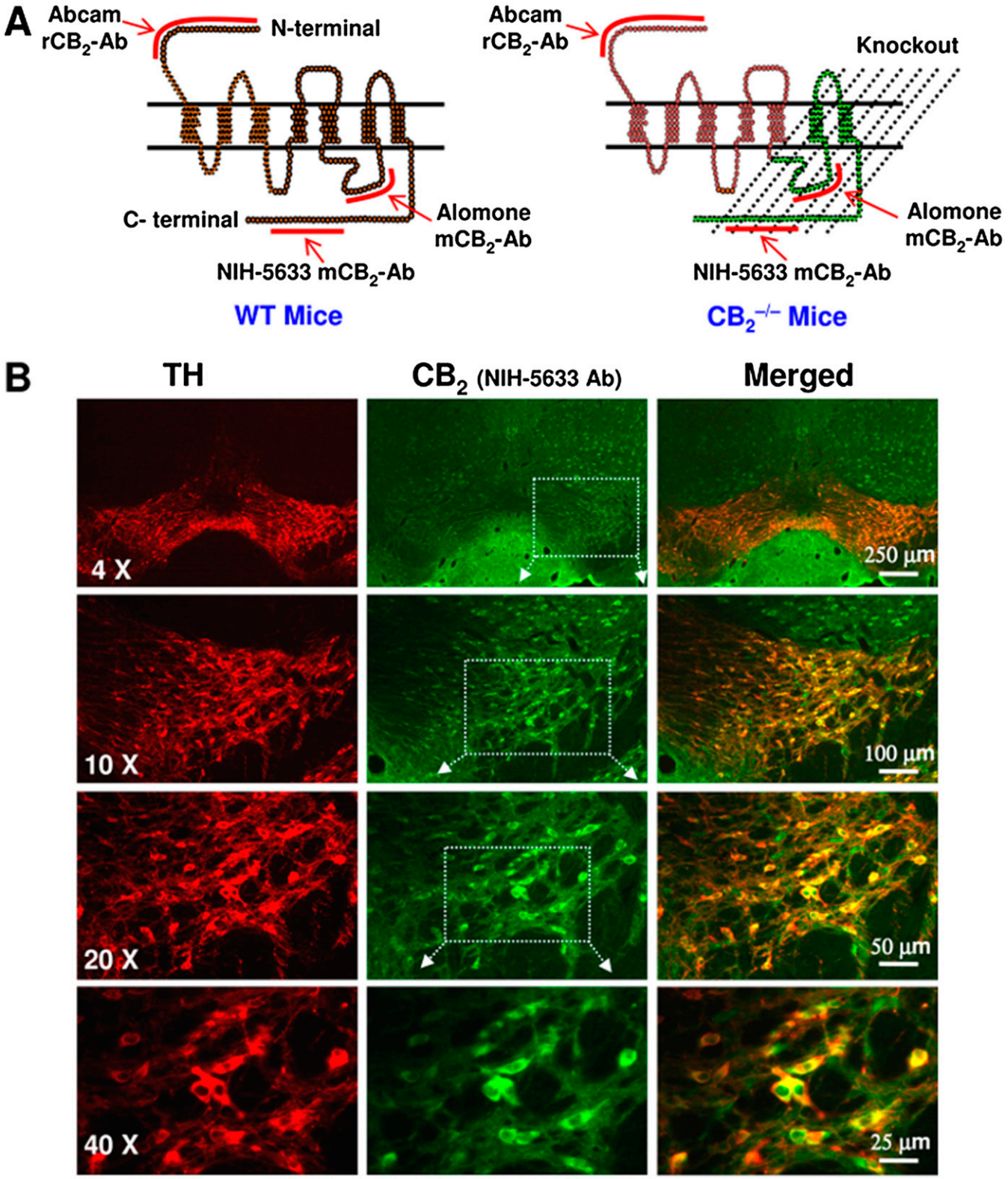

Fig. S2. (Related to Fig. 3.) CB_2R immunostaining as detected in midbrain VTA DA neurons. (*A*) Diagrams showing mCB_2R structures in WT and $CB_2^{-/-}$ mice, deleted receptor region of CB_2Rs in $CB_2^{-/-}$ mice, and the binding sites on mCB_2Rs of the three antibodies used in the present study. (*B*) Representative IHC images under different magnifications in WT mice, illustrating mCB_2R immunostaining in VTA DA neurons (yellow in the merged images) and also in non-DA VTA neurons (green in the merged images).

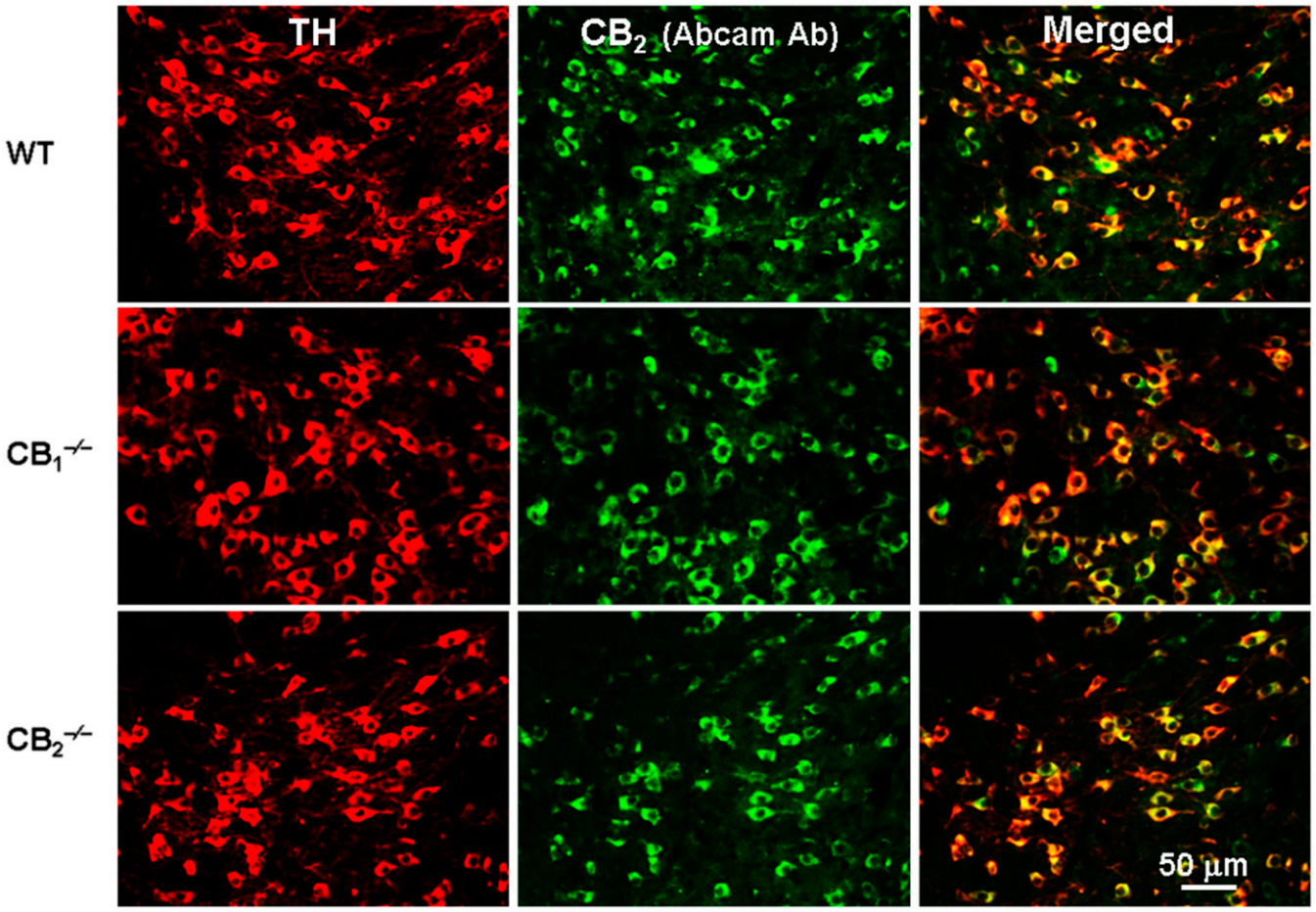

Fig. S3. (Related to Fig. 3.) CB_2R immunostaining in the VTA, illustrating that the Abcam antibody with eiptope at the extracellular N terminal detected similar densities of CB_2 staining in VTA DA neurons in WT, $CB_1^{-/-}$, and $CB_2^{-/-}$ mice.

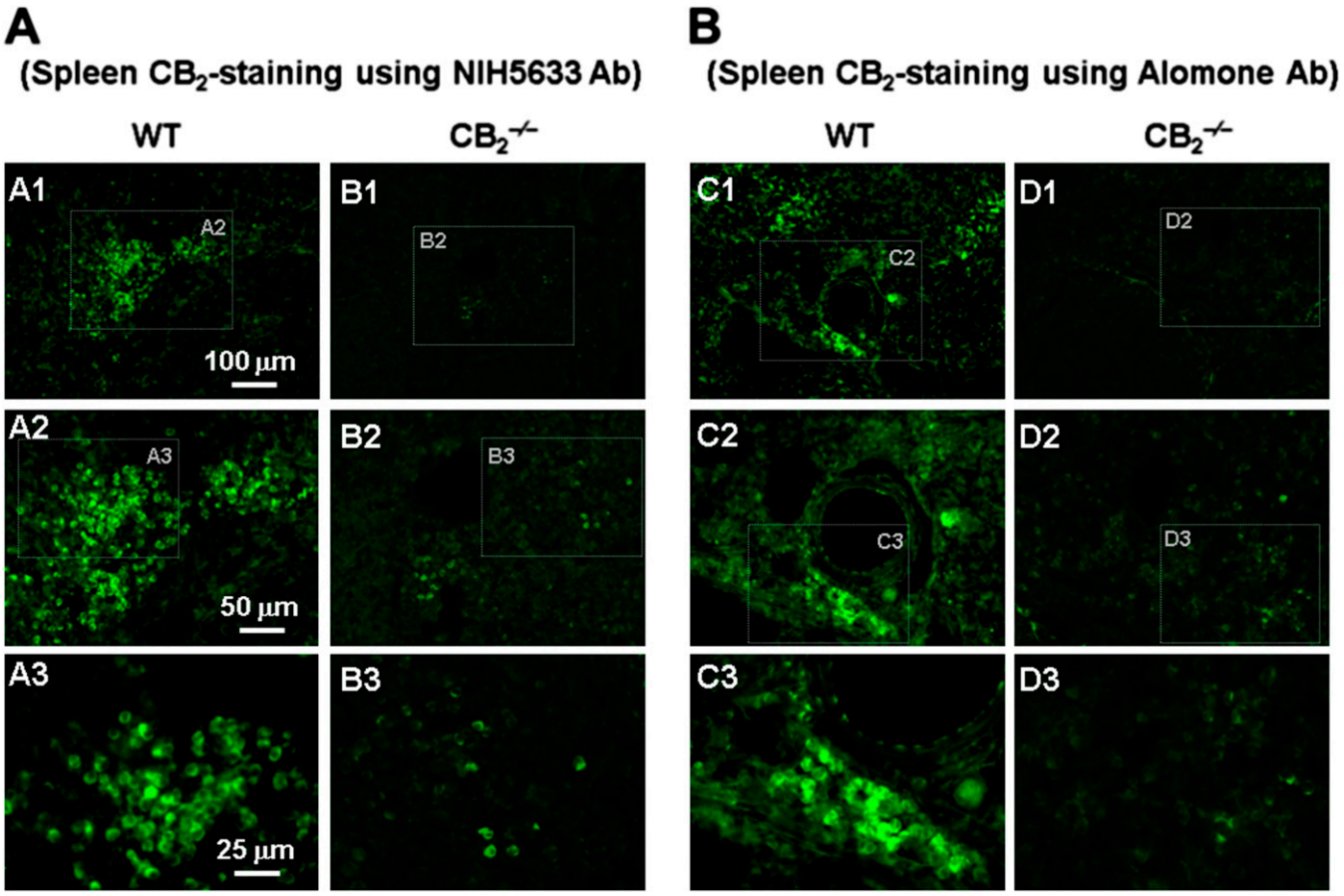

Fig. S4. (Related to Fig. 3.) CB_2R immunostaining in spleen tissue. The NIH5633 (*A*) and Alomone (*B*) antibodies detected high densities of CB_2R staining in splenocytes of WT mice, but low densities of staining in Zimmer $CB_2^{-/-}$ mice.

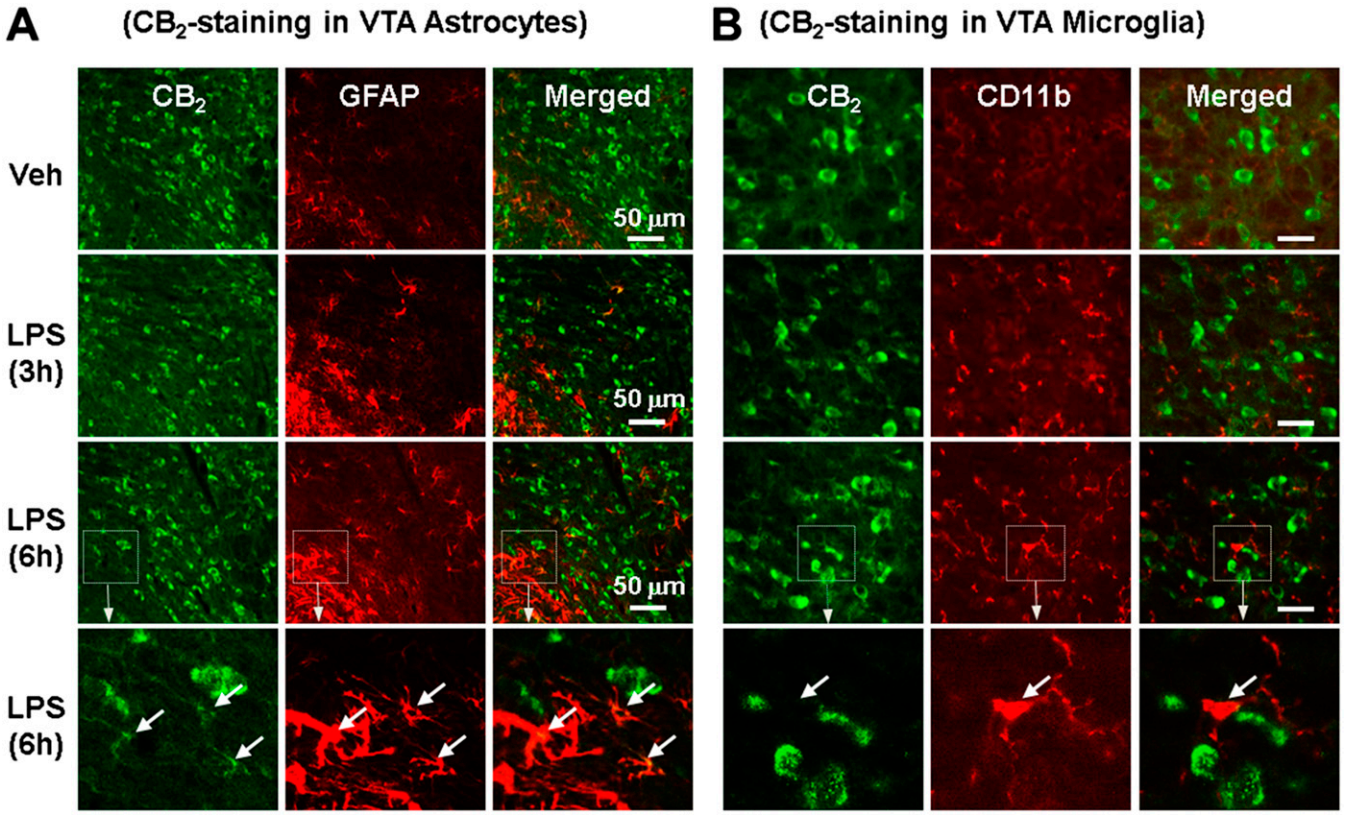

Fig. S5. (Related to Fig. 3.) CB_2R immunostaining in glial cells. Low density of CB_2R staining was detected in GFAP-labeled astrocytes (*A*), but not in CD11b-labeled microglia (*B*) in saline or lipopolysaccharide (LPS)-treated WT mice.

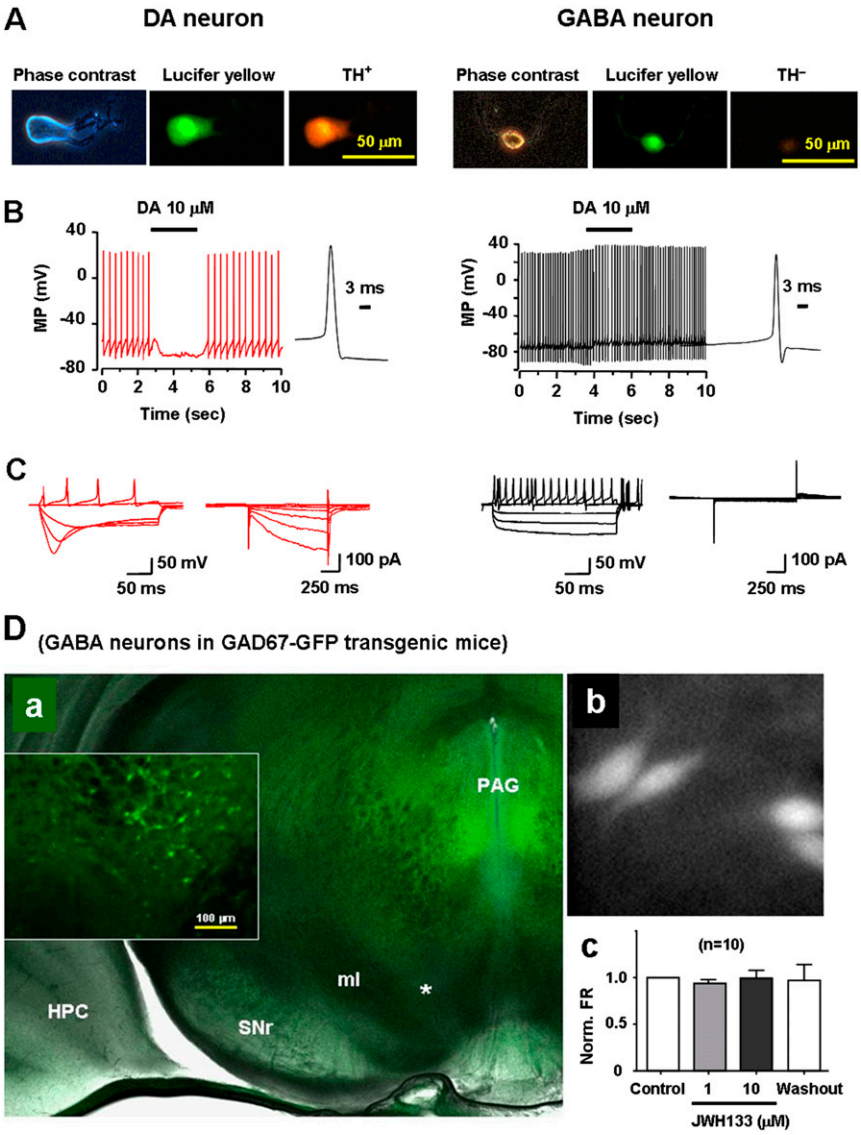

Fig. S6. (Related to Fig. 4.) Experimental methods used to identify VTA DA and GABA neurons. (*A*) Images showing VTA DA and GABA neurons before (phase-contrast images) and after (Lucifer yellow-labeled images) patch-clamp whole-cell recording. IHC staining shows that DA neurons were TH-positive (TH^+), whereas GABA neurons were TH-negative (TH^-). (*B*) Bath-applied DA inhibited firing of VTA DA neuronal firing (*Left*), but not of VTA GABA neurons (*Right*). VTA DA neurons exhibited low firing rates (1–3 Hz) with relatively long action potential durations, whereas VTA GABA neurons exhibited high firing rates (>7 Hz) with short action potential durations. (*C*) VTA DA neurons usually showed a characteristic H-current, whereas VTA GABA neurons did not. (*D*) Effects of JWH133 on VTA GABAergic neurons. (*D*, *a*) Representative fluorescence microscopy pictures of VTA GABA neurons prepared from GAD67-GFP transgenic mice. (*Inset*) Enlarged view showing GAD67-positive neurons (GABA neurons) in the VTA (VTA location indicated by asterisk). (*D*, *b*) A representative differential interference contrast (DIC) image with fluorescence filter, in which GAD67-positive neurons are bright and can be selected for patch-clamp recording. (*D*, *c*) JWH133 (1; 10 μM for 10 min) did not alter GABA neuronal firing in VTA slices. MP, membrane potential; Norm. FR, normalized firing rate.

Table S1. MGB TaqMan probes and primers used for qRT-PCR assays (related to Fig. 1)

	MGB TaqMan probe	Forward primer	Reverse primer
mCB_{2A}	CTGACAAATGACACCCAGTC	CAGGACAAGGCTCCACAAGAC	GATGGGCTTTGGCTTCTTCTAC
mCB_{2B}	TGGGCCCAGTCTT	GCCACCCAGCAAACATCTCT	GATGGGCTTTGGCTTCTTCTAC
CB_2-KO	ATGCTGGTTCCCTGCAC	AGCTCGGATGCGGCTAGAC	AGGCTGTGGCCCATGAGA
β-actin	ATGAAGATCAAGATCATTGCT	GATTACTGCTCTGGCTCCTAGCA	CCACCGATCCACACAGAGTACTT

Table S2. Effects of JWH133 (1 μM) on AP parameters in dissociated VTA DA neurons (related to Fig. 4)

Treatment	RP, mV	AP initiation, ms	AP width, ms	AHP 1, mV	AHP 2, mV	FR, Hz
Control	–42.7 ± 3.1	15.0 ± 2.1	2.43 ± 0.13	38.8 ± 3.9	21.3 ± 2.2	3.0 ± 0.1
JWH133	–51.4 ± 0.5*	50.6 ± 4.9†	2.10 ± 0.11*	46.6 ± 3.1*	25.0 ± 3.8	2.3 ± 0 0.2*
Wash	–42.8 ± 4.7	12.3 ± 3.3	2.41 ± 0.14	38.3 ± 4.2	18.2 ± 3.1	2.9 + 0.2

These data were collected from 11 VTA DA neurons from six mice. *$P < 0.05$; †$P < 0.01$, paired *t* test (compared with control). These results show that JWH133 (1 μM) significantly hyperpolarizes resting membrane potential, retards AP initiation, reduces AP duration, enhances AHP amplitude, and reduces neuronal FR. RP, resting potential; AP, action potential; AHP, afterhyperpolarization potential; FR, firing rate.